

Three-Dimensional Force Profile During Cochlear Implantation Depends on Individual Geometry and Insertion Trauma

Ersin Avci,¹ Tim Nauwelaers,² Volkmar Hamacher,² and Andrej Kral¹

Objectives: To preserve the acoustic hearing, cochlear implantation has to be as atraumatic as possible. Therefore, understanding the impact of the cochlear geometry on insertion forces and intracochlear trauma might help to adapt and improve the electrode insertion and reduce the probability of intracochlear trauma.

Design: The study was conducted on 10 fresh-frozen human temporal bones. The inner ear was removed from the temporal bone. The bony capsule covering the scala vestibuli was removed and the dissected inner ear was mounted on the three-dimensional (3D) force measurement system (Agilent technologies, Nano UTM, Santa Clare, CA). A lateral wall electrode array was inserted, and the forces were recorded in three dimensions with a sensitivity of 2 μ N. Afterwards, the bones were scanned using a Skyscan 1173 micro-computed tomography (micro-CT). The obtained 3D force profiles were correlated with the videos of the insertions recorded through the microscope, and the micro-CT images.

Results: A correlation was found between intracochlear force profiles measured in three different directions with intracochlear trauma detected with micro-CT imaging. The angle of insertion and the cochlear geometry had a significant impact on the electrode array insertion forces and possible insertion trauma. Intracochlear trauma occurred frequently within the first 180° from the round window, where buckling of the proximal part of the electrode carrier inside the cochlea, and rupturing of the spiral ligament was observed.

Conclusions: The combination of the 3D force measurement system and micro-CT can be used to characterize the mechanical behavior of a CI electrode array and some forms of insertion trauma. Intracochlear trauma does not always correlate with higher force amplitudes, but rather with an abrupt change of force directions.

Key words: Cochlear implant, Electrode, Hearing preservation, Insertion force, Insertion trauma, μ CT, Round window, Scala tympani.

(Ear & Hearing 2016;XX;00–00)

INTRODUCTION

Cochlear implants (CIs) are a standard treatment of severe to profound sensorineural hearing loss. Subjects with good residual hearing in the middle to low frequencies but poor speech understanding can benefit from a combination of electrical stimulation through the CI and amplification of residual acoustic hearing (electric-acoustic stimulation). The addition of acoustic low frequency amplification has shown to provide better speech perception over electrical stimulation only (von Ilberg et al. 1999; Gantz & Turner 2004; Kiefer et al. 2005; Lenarz 2009).

To preserve the acoustic hearing, cochlear implantation has to be as atraumatic as possible. One of the most critical point

during surgery is the opening of the cochlea (the cochleostomy) and the insertion of the CI electrode carrier into the scala tympani (ST). There are three factors that influence the electrode insertion: cochlear anatomy, surgical approach, and electrode design. It is well known that the cochlea shows considerable interindividual variability in size and morphology (Zrunek & Lischka 1981; Kawano et al. 1996; Wysocki 1999; Escudé et al. 2006; Erixon et al. 2009; Biedron et al. 2010; Verbist et al. 2010; Rask-Anderesen et al. 2011; Shin et al. 2013; Avci et al. 2014). Therefore, the actual dynamics of an electrode array insertion is likely different from subject to subject. This opens the question whether the amount of intracochlear trauma during electrode array insertion depends on the individual variability of the human cochlea. Obviously, also the experience of the surgeon has an influence on the implantation (Aschendorff et al. 2007; Franke-Trieger et al. 2014; Rohani et al. 2014; Wade et al. 2014; Wanna et al. 2014). Today, implantation is performed either through the round window (RW) or through a separate cochleostomy. Due to the absence of any visualization of the intracochlear duct and intracochlear structures during implantation, the electrode array is inserted blindly and is only guided by tactile feedback. What remains unclear is whether the insertion force and speed can predict the probability of intracochlear trauma. For this, precise force measurements and correlation to implantation trauma are required.

Usually, the surgeon inserts the electrode array until felt resistance is encountered. Limited data about intracochlear forces generated by the electrode insertion are available. One-dimensional force measurement systems (FMSs) have been used to evaluate new electrode prototypes (Radeloff et al. 2009; Briggs et al. 2011; Helbig et al. 2011; Nguyen et al. 2012; Kobler et al. 2015) or to estimate the amount of force applied to the intracochlear structures (Majdani et al. 2010; Rau et al. 2010; Schurzig et al. 2010; Kontorinis et al. 2011; Miroir et al. 2012; Schuster et al. 2015). However, to the authors' knowledge, no study investigated the impact of the cochlear anatomy on insertion forces and intracochlear trauma. Understanding the impact of the cochlear geometry on insertion forces and intracochlear trauma might help to adapt and improve the electrode insertion and reduce intracochlear trauma overall. Such experiments cannot be performed in living subjects.

The present study used an advanced and sensitive three-dimensional (3D) FMS and an automatic insertion to investigate implantation forces. Cadaver temporal bones have been used. The study demonstrates that force profiles depend on the cochlear geometry and that they are well reproducible in the same cochlea provided the same insertion angle is guaranteed. The outcomes provide evidence of a relation between some forms of trauma and cochlear anatomy. However, forces potentially related to intracochlear trauma were in most cases below the sensitivity of a human hand.

¹Cluster of Excellence Hearing4all, Institute of AudioNeuroTechnology and Department of Experimental Otolology, Ear, Nose, and Throat Clinics, Hannover Medical University, Hannover, Germany; and ²Advanced Bionics, European Research Center, Hannover, Germany.

MATERIALS AND METHODS

Preparation of Human Temporal Bone

For the present study, 10 fresh-frozen human temporal bones (fixed with 1% formaldehyde) without any evidence of malformations were used. Five were left and five were right temporal bones. To preserve the integrity of the microanatomy of the cochlea, the bones were thawed at room temperature (Rosowski et al. 1990; Ravicz et al. 2000). Subsequently, the cochlea was isolated from the temporal bone. To obtain a clear view of the osseous spiral lamina (OSL), basilar membrane (BM), and the underlying ST, the bony capsule covering the scala vestibuli (SV) was removed (Fig. 1B). The opening of the otic bony capsule was performed using a 0.5 mm diamond burr at low speed (Karl Storz, Tuttlingen, Germany). The bony overhang of the RW niche was completely removed by a diamond burr (0.5 mm). The RW membrane was fully exposed (using a needle), and the anteroinferior edge was carefully drilled away. To remove possible bone dust inside the ST, the cochlea was several times carefully rinsed with 0.9% saline using a syringe with a long needle at the RW opening. All cochleae were checked under a digital microscope (VHX 5000, Keyence corporation, Osaka, Japan), where no damage of the microanatomy was observed attributable to preparation and fixation.

Electrode Array Insertion With a Three-Dimensional Force Measurement System

Insertion forces were recorded by a 3D FMS (Nano UTM, Agilent technologies, Santa Clara, CA; Fig. 1A). The three dimensions enables to measure forces in the direction of insertion (z force; Fig. 1B), in the cochlear vertical plane (y force), and in the direction orthogonal to “ z ” and “ y ” (x force; Fig. 1C). The FMS consists of a nanomechanical actuating transducer (load resolution: 50 nN; dynamic range: 0.1 Hz to 2.5 kHz) and a robotic extension arm with a rod pusher that guides the electrode array through the insertion tube into the cochlea (0.5 $\mu\text{m/s}$ to 5 mm/s). The lateral forces (F_x and F_y) were measured through optical interferometry with a resolution of 2 μN . The insertion procedure was recorded in real-time with a high-resolution CCD camera (DXC-390, Sony, Tokyo, Japan) connected to a surgical microscope (OPMI ORL, Carl Zeiss, Jena, Germany). The microdissected cochlea was mounted using a custom-made holder on the FMS. The electrode array was loaded into an insertion tube, and the electrode tip was placed adjacent to the RW. It was necessary to avoid touching the edge of the RW so that no external forces from the insertion tube act on the cochlea. Therefore, a second camera (DigiMicro 2.0, dnt, Dietzenbach, Germany) recorded the RW opening. The cochlea was filled with 0.9% saline solution. The electrode array was inserted with a constant velocity of 0.5 mm per second as performed in most previous studies (Radeloff et al. 2009; Helbig et al. 2011; Miroir et al. 2012; Nguyen et al. 2012; Kobler et al. 2015), and the forces were captured every 30 msec. The insertion was terminated as soon as the electrode tip stopped advancing. In cases without trauma to the BM or OSL (observed through the insertion video), the insertion was repeated three times, with the same setup and the same electrode. After each insertion, the electrode array was cleaned with distilled water to remove any proteins on the surface of the electrode.

To avoid the mechanical variability of different electrode arrays, only one type of electrode array was used. We used a

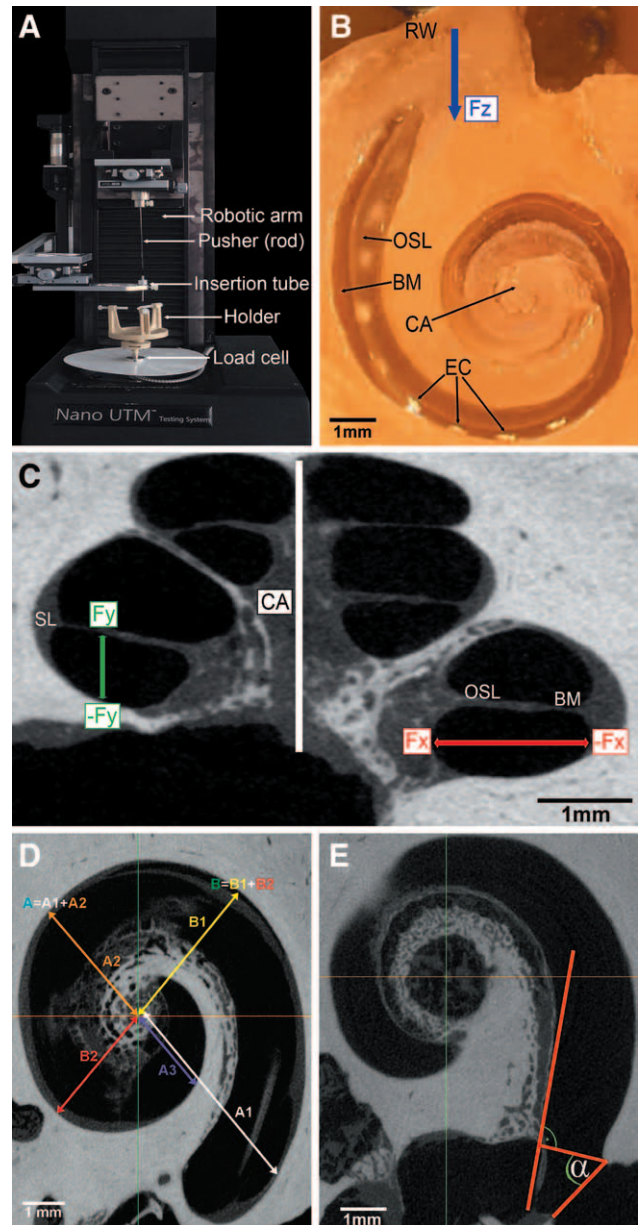


Fig. 1. A, The cochlea was mounted on the force measurement system and the insertion forces were recorded. The insertion axis was tangential to the basal part of the ST and in alignment to the z axis of the force measurement system. The insertion procedure and the forces were automatically recorded in real-time, whereas the camera for recording the movement of the electrode array was positioned perpendicular to the plane of insertion. B, Cochlear dissection showing a lateral wall electrode in contact with the lateral wall of the ST. Electrode contacts are clearly visible through the OSL and basilar membrane. C, The micro-CT image of an air-filled human cochlea (resolution: 10 μm). X force represents the force against the lateral (positive) or modiolar wall (negative). Y force represents the force into the direction of the SV (basilar membrane, OSL, spiral ligament) (positive) or scala floor (negative). Micro-CT image of a cochlea in axial view (D and E). D, The two lines divide the first turn in four quadrants. The length A is the sum of $A_1 + A_2$ (A_3 is part of A_1), whereas the width B is the sum of $B_1 + B_2$. E, A line was drawn tangentially to the modiolar wall of the basal part, and orthogonal to this line to this inferior edge of the RW, whereas α is the angle between the orthogonal line and the superior edge of the RW. BM indicates basilar membrane; CA, central axis; CT, computed tomography; EC, electrode contacts; OSL, osseous spiral lamina; RW, round window; ST, scala tympani; SV, scala vestibuli.

research electrode array of the same design as the HiFocus 1J from Advanced Bionics. All parameters and dimensions were identical with the HiFocus 1J. It had a proximal diameter of 0.8 mm, and a distal diameter of 0.4 mm with a total length of 19.75 mm.

Scanning, Segmentation, and Dimensional Analysis

After implantation, the cochlear fluid was gently removed at the RW using a suction tube. Great care was given not to apply the full negative pressure of the suction tube (near <5 kPa) to the cochlear spaces. Instead we did so at some distance from the cochlea only to remove the fluid inside of the ST by help of water adhesion. Then, the cochleae were wrapped with formaldehyde-immersed cotton tissue for fixation of the fragile structures. Subsequently, they were scanned by using a high energy micro-computed tomography (CT) device (Skyscan 1173, Bruker, Kontich, Belgium), which is described elsewhere (Avci et al. 2014), giving an isotropic voxel size of 10 μm .

Mimics Innovation Suite software (version 17.0, Materialise, Leuven, Belgium) was used to segment out the cochlea, ST, and RW from each of the image datasets. Based on these segmentations, 3D reconstructions of each cochlea were created. Cross-sectional images were used to measure the internal dimensions of the ST. Slices were taken every 0.1 mm orthogonal to the lateral wall of the ST. The image slices were exported and analyzed by a custom-made software in MATLAB (MathWorks, Natick, MA). The software calculated the cross-sectional diameter, the area of the ST, and the vertical trajectory of the 10 scalae (Avci et al. 2014).

Basic cochlear measurements were realized with Mimics Innovations Suite (Fig. 1D). Two construction lines were drawn: one line from the midpoint of the RW through the central axis to a distant point of the first turn, and the other one orthogonal to the first one through the central axis. These lines divided the first turn into four quadrants. In addition, RW angle relative to ST was measured (Fig. 1E). For this purpose, a line was drawn tangential to the modiolar wall of the basal part, and orthogonal to this line to the inferior edge of the RW, whereas α is the angle between the orthogonal line and the superior edge of the RW.

Data and Statistical Analysis

Analysis of the generated force profiles was organized using Excel (Microsoft, Redmond, WA). The spread sheets contain the forces for each insertion including insertion time, insertion distance, and insertion forces (x , y , and z). Insertion distance was calculated based on the duration of insertion at predefined speed. Because there was no obvious difference in the data for left and right cochleae, to facilitate the comparison of the x forces, data from the left ears have been spatially mirrored. For each cochlea, the mean insertion force for each direction was calculated by averaging the recorded data of three insertions. The insertion videos were analyzed and cut using Windows Movie Maker (Microsoft). The angular distance was defined using video images, whereas a line connecting the center of the long diameter of the RW and the central axis was the reference line (0° reference angle). Each insertion forces were analyzed, and related to the corresponding insertion video. Electrode buckling or kinking, dislocation from the scala, or lifting of the BM were documented and the degree of trauma were checked using the micro-CT data, using a scale of 0 to 4 (modified from

Eshraghi et al. 2003). Furthermore, the cochlear geometry and the mean insertion forces were correlated.

Statistical testing was performed by one-way analysis of variance and regression analysis. p values of <0.05 were considered statistically significant.

RESULTS

In this study, 10 cochleae were used, where a total of 27 insertions was analyzed. The goal was to correlate CI insertion forces with insertion trauma. Moreover, the impact of the cochlear geometry on insertion forces was investigated. Micro-CT provided exact measurements of the cochlear dimensions before insertion.

The analysis of the basic anatomical cochlear parameters (Table 1) revealed coefficient of variation between 3 and 10%.

Repeatability

To define the optimal insertion speed for the measurements, the influence of seven different speeds on the force profile was tested on an artificial 3D model of a human cochlea. The model was created by scanning a human cadaveric bone that well represented the mean values of size and wrapping (Avci et al. 2014). To obtain an exact replica of the ST this bone was segmented. The material used for the model was acrylic polymer, which was filled with 10% soap solution, and allowed smooth insertions. Insertion speed measurements revealed no significant variation in insertion forces for speeds between 0.05 and 2 mm/s. The mean z forces for insertion speed from 0.05 to 2 mm per second were 16.4 to 19.2 mN, and maximum forces were from 41.5 to 53.0 mN. The insertion speed 0.5 mm per second was chosen for the temporal bone measurements because it was comparable with the majority of previous studies. In what follows, the CI electrode array was inserted using an automatic insertion tool with a constant speed of 0.5 mm per second, and the forces were captured every 30 msec.

The repeatability of the insertion procedure was evaluated by multiple electrode array insertion on a freshly microdissected human cochlea. The cochlea was mounted on the FMS and was filled before each insertion with 0.9% saline. The same electrode array was inserted three times through the RW into the ST. The cochlea and the electrode array were cleaned after each insertion with distilled water. The 3D FMS allowed repeatable measurements with largest forces found in the z direction (the direction of insertion), well reproducible within one temporal bone, the same setting and the same electrode array (Fig. 2). The maximum SD in the range from 90° to 180° was 3 mN (12 ± 3.4 mN), the maximum measured SD for the complete insertion was 28 mN (300 ± 28 mN). The mean coefficient of variation from the initial contact between the electrode tip and the lateral wall up to the end of the insertion was below 12%, whereas largest coefficients were observed within the first 10 mm and between 14.5 and 16.5 mm. This result was typical for all repeated insertions.

Three-Dimensional Force Profile Characteristic

First, we report one typical insertion profile obtained in one temporal bone (Fig. 3). Here, the measured forces and snapshots from visual control are provided in the same figure to allow correlating forces to the parallel electrode insertion

TABLE 1. Measurement of the cochlear partitions with mean and SD for 10 cochleae

Cochlea	A (mm)	A1 (mm)	A2 (mm)	A3 (mm)	B (mm)	B1 (mm)	B2 (mm)	RW Angle (°)
1	9.44	6.28	3.16	2.45	6.71	3.93	2.78	63.9
2	9.29	6.25	3.04	2.36	7.08	4.20	2.88	67.0
3	9.15	5.87	3.28	2.47	6.95	4.06	2.89	66.1
4	9.53	5.92	3.61	2.61	7.54	4.32	3.22	60.0
5	9.00	5.65	3.35	2.44	6.84	4.04	2.80	60.6
6	9.56	5.99	3.57	2.53	7.63	4.77	2.86	63.4
7	9.06	5.87	3.19	2.20	6.75	3.94	2.81	50.3
8	9.20	5.99	3.21	2.39	6.90	4.13	2.77	68.0
9	9.20	6.11	3.09	2.38	6.68	3.93	2.75	55.7
10	10.03	6.50	3.53	2.60	7.32	4.25	3.07	56.1
Mean	9.35	6.04	3.30	2.44	7.04	4.16	2.88	61.1
SD	0.31	0.25	0.20	0.12	0.34	0.26	0.15	5.7

RW, round window.

process. During the electrode insertion, the *z* force started to rise with the first contact, when the electrode tip touched the lateral wall of the ST (position I), followed by an increase of the *x* force against the lateral wall of the basal part (Fig. 3). Then, the electrode array tip started to bend, and engaged with the lateral wall. From that point on (II), the *z* force started to rise again, and the *y* force started to increase or (in some temporal bones, not shown) decrease, depending on the vertical trajectory of the cochlea (II). As the electrode array was inserted further, the middle part of the electrode array engaged with the lateral wall (II to III), and another significant rise in the *z* direction was observed (III). Finally, the proximal part of the electrode array started to engage with the lateral wall (III to IV), and the final rise in the *z* direction occurred (IV).

Typically, with the current setup, the electrode array did not touch the intracochlear structures during the first 8 mm of the insertion. Correspondingly, the forces in all three directions did not change significantly in the first 8 mm insertion. Subsequently, after the first contact with the cochlear wall, the proximal part of the electrode carrier started pushing toward

the lateral wall, leading to a substantial increase of the insertion force (points II, III, and IV) due to the increased friction.

The visual control revealed a relation of the forces with subsequent cochlear trauma in a 3D force profile, particularly in the *x* force (Fig. 3). The *x* force slightly increased near 11 mm as the electrode carrier was pushing toward the lateral wall, owing to increased contact between the electrode carrier and the lateral wall (Fig. 3). Afterwards, near 18 mm, the *x* force decreased suddenly while the *y* force increased. This force profile appeared synchronous to visually-detected electrode buckling. This sudden decrease of the *x* force occurred thus indicated buckling of the proximal part of the electrode carrier. The proximal part of the electrode carrier folded (partly) into an inferior or superior direction, which might have caused additional trauma to the endosteum, spiral lamina, or the modiolar wall of the ST.

To support this interpretation, all the *x* force profiles with electrode buckling were synchronized to the moment of buckling (Fig. 4A), revealing that in seven (70%) of the cochleae a drop of the *x* force occurred with buckling. The *y* forces were small. A sudden increase of the *y* force typically indicated a

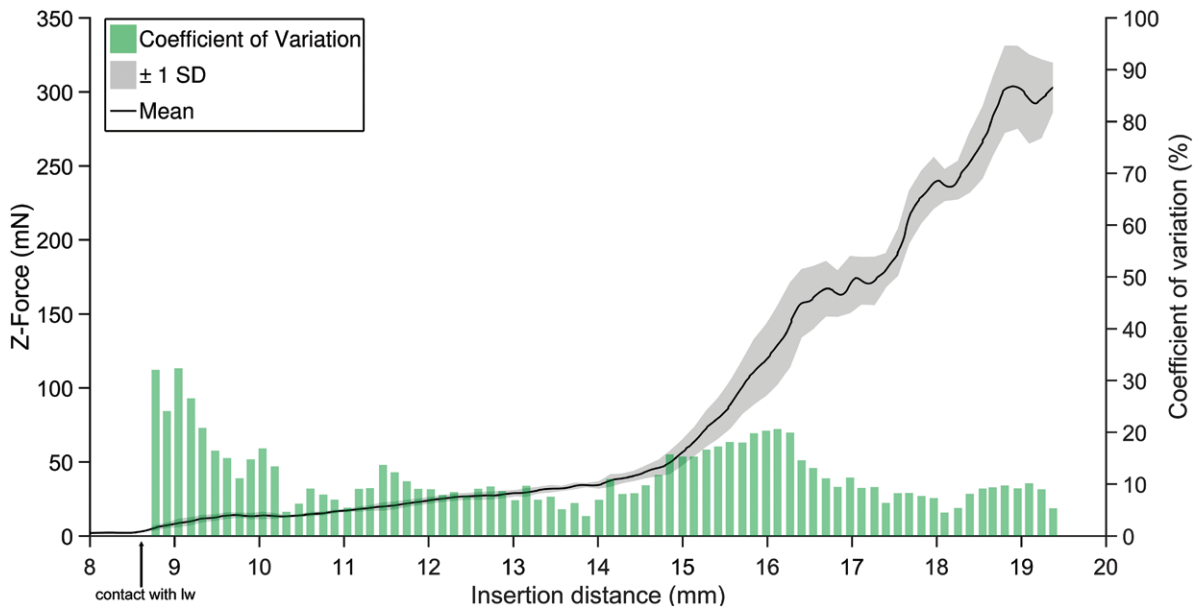


Fig. 2. Mean force profile over three implantations (black) with ± 1 SD (grey) as a function of insertion distance (left y axis). The green bars represent the coefficient of variation (right y axis). LW, lateral wall.

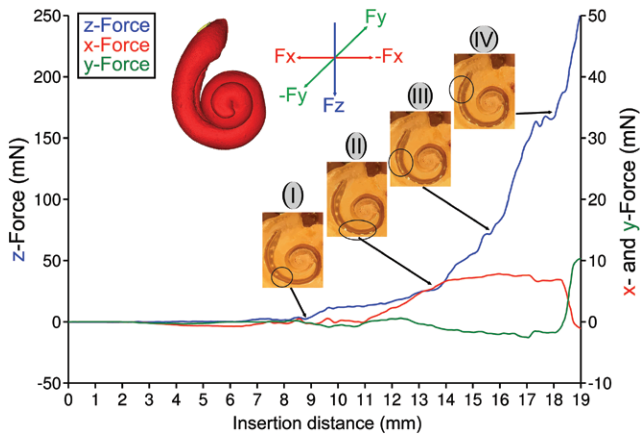


Fig. 3. Typical mean force profile of three insertions as a function of insertion distance. Insertion distance was calculated based on the duration of insertion at predefined speed. Blue line shows the z force (left y axis), red line the x force, and green line the y force (right y axis). Force profile started to increase with the first contact with the lateral wall. The circles in each of the images (I–IV) indicate the part of the electrode array that starts to engage with the lateral wall. The electrode array started to buckle at 18.5 mm, where a sudden change of the x and y forces occurred.

movement of a part of the electrode carrier toward the scala vestibuli/scala media or the scalar floor. A sudden increase of the y force was observed in all but one cochleae simultaneously with the occurrence of buckling of the proximal part of the electrode carrier (Fig. 4B), whereas the carrier tended to move into the direction of the SV/SM, and caused trauma at the level of the BM/OSL. Using these two force components, x and y , thus allowed to predict buckling in all the cases when it occurred by either a decrease of x force or an increase in y force (or both). However, only in 5 of 10 cases a sudden increase of the z force was observed.

All z forces from the 10 cochleae were merged at initial contact between the electrode tip and the lateral wall of the cochlear basal near 7 mm insertion depth (Fig. 5). As the electrode carrier moved further along the lateral wall of the ST, the anatomical variability of the cochleae had a larger impact on the friction force (z force), whereas significant variability was observed at around 12.8 ± 1 mm ($197^\circ \pm 25^\circ$) from the RW.

The mean insertion depth of the 10 cochleae was 18.8 ± 0.6 mm ($327^\circ \pm 22^\circ$). Consequently, the insertions were in essence full insertions. The initial contact between the electrode tip and lateral wall of the basal part was 8.1 ± 0.6 mm ($121^\circ \pm 9^\circ$). The mean maximum z force was 218 ± 44 mN. The mean maximum y force was on average 25.0 ± 12.2 mN, and 19.5 ± 8.6 mN for the maximum x force.

Largest forces occurred in z direction. We calculated the amount of the x and y force relative to the z force. In mean, the x force was 13% of the z force, whereas the y force was only 8.5% of the z force. Moreover, we found statistically significant correlations between the forces: If the contact between the electrode tip and the lateral wall of the ST occurred earlier, the maximal measured y force was higher ($R^2 = 0.70$). Furthermore, the x force started to rise simultaneously with initial contact between electrode tip and lateral wall of the ST ($R^2 = 0.82$), and increased up to 180° parallel with the z force ($R^2 = 0.73$).

Thus, the z force was best reflecting the insertion process and the amount of contact of the electrode array with the lateral

wall, likely reflecting friction. The x - and the y forces, on the other hand, predicted the electrode buckling and thus its deviation from the standard insertion direction. This supports the idea that measurements in all directions are necessary to fully describe the insertion process and monitor implantation.

Insertion Trauma

While rupture of the BM was observed in most cases visually during insertion, more detailed analysis postinsertion was performed with micro-CT scans. These demonstrated trauma to the BM in three of seven cochleae and a rupture of the spiral ligament (SL) in six of seven cochleae (Fig. 6A, B). Intracochlear trauma occurred frequently within the first 180° from the RW (Fig. 6C, D), where buckling of the proximal part of the electrode carrier inside the cochlea was observed. Rupture of the SL occurred between 35° and 170° from the RW. In cases where SL rupture occurred, the mean maximal x force was 2.5 times higher compared with insertions where SL remained intact (23.7 mN compared with 11.3 mN). Furthermore, in two temporal bones, rupture of the SL started subsequently after BM trauma. Interestingly, there was no case where BM and SL rupture occurred at the same location. Moreover, combined analysis of the micro-CT and video recording revealed no trauma caused by the electrode tip in the present experiments (with given insertion angle and speed). Other insertion angles, however, may cause additional trauma at the tip, too.

An important aspect is whether it is possible to detect trauma by identification of how force profiles change over insertion depth. Figure 7 shows a case where the first insertion in this cochlea was without visually-detected trauma, where buckling was mild and just initiated at the very end of the insertion (insertion depth of 18.9 mm from the RW). During the second insertion, however, buckling of the proximal part of the electrode array lifted the BM (observed in visual control), starting already at an insertion depth of 17 mm (276°) from the RW. As can be seen in Table 2, and Figure 7, the total insertion force was lower in case where intracochlear buckling and stronger BM lifting was observed (lower x and z forces, higher y forces). Moreover, the occurrence of trauma was indicated by a sudden change in force direction in the second insertion (drop in x force and increase in y force). This case demonstrates that the forces in implantation when trauma occurred must not necessarily be higher—partly even lower—compared with cases with no trauma. The contribution of the z force reflects the friction between the electrode array and the lateral wall of the ST, where a reduction of the total force would be an indication of electrode dislocation (as seen in Fig. 7). Sudden change of the x force or sudden increase/decrease of the y force may thus indicate the risk of insertion trauma. However, this does not implicate that implantations with low forces are more likely to cause more trauma, on the contrary. As we will show next, total forces reflect the shape of the cochlea and this is a factor in implantation trauma. If trauma does occur, the z force tends to drop because forward movement of the electrode is rerouted and thus does not reflect the friction of the implant with the lateral wall any more.

Correlation Between Cochlear Geometry and Force Profile

Furthermore, force profiles during implantation revealed correlations with cochlear geometry and the surgical approach.

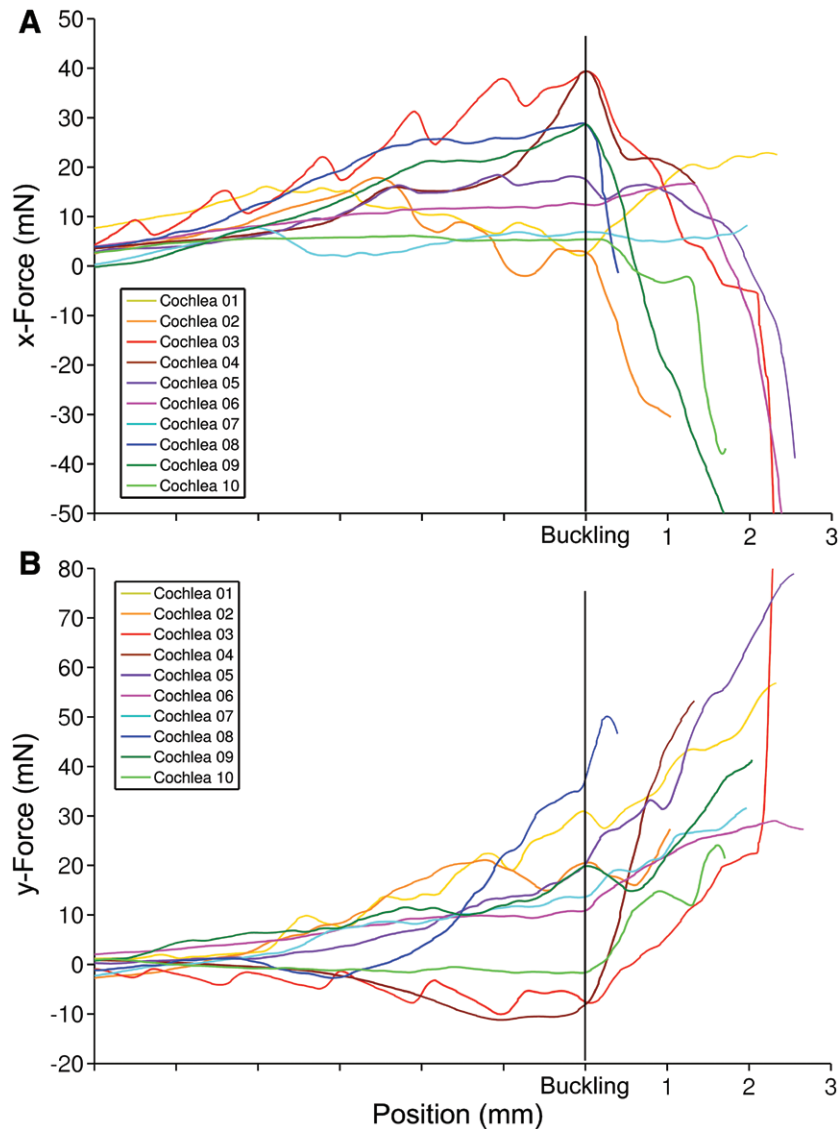


Fig. 4. The individual x and y forces of the 10 cochleae as a function of the insertion distance (A and B). The x and y forces are merged to where the electrode carrier started to buckle. In cases of buckling, 7 of 10 cochleae showed a sudden change of the x force (A), whereas in 6 of 10 cochleae, a sharp increase of the y force occurred (B).

Figure 8A shows the relation between the RW angle and the z force. If the angle of the RW was large, and the insertion vector pointed more toward the modiolar wall, then the z force increased more ($R^2 = 0.75$, Fig. 8A). This can be explained by the fact that a higher RW angle causes the electrode array to hit the lateral wall in a more orthogonal direction opposed to more tangential, leading to higher resistance. In consequence, the insertion angle, as defined in Figure 8A, should be kept as small as possible.

The angle of the initial contact between the electrode tip and the lateral wall (straight: 59.6° ; angled: 64.8°) had also an impact on the initial increase of the z force (Fig. 8B). A straight touch of the electrode tip with the lateral wall led to higher slope of the z forces (23 mN/mm), whereas the slope of an angled touch was twice as low (slope: 11 mN/mm).

Moreover, the cochlear size had a substantial influence on the force profiles. There was a significant positive correlation between lengths A , A_2 , and B and forces. Larger A_2 values

lead to higher mean z forces between 90° and 180° ($R^2 = 0.63$), where cochleae with a sharp shape at the basal part leads to have an increased z force at that region. The z forces between 180° and 270° were higher with larger A values ($R^2 = 0.51$). Larger cochleae lead to longer distance along the lateral wall (one cochlear turn) ($R^2 = 0.87$), whereby the increase in z force was higher between 90° and 180° for longer cochleae ($R^2 = 0.61$). The angular distance was lower for larger cochleae ($R^2 = 0.50$), whereas the electrode insertion distance was longer until 270° ($R^2 = 0.77$).

DISCUSSION

The present study is the first report on the 3D force measurement analysis of the mechanical behavior of the CI electrode during implantation. The force profiles measured in three different directions could be well correlated with intracochlear trauma detected with micro-CT imaging. The angle of insertion and the

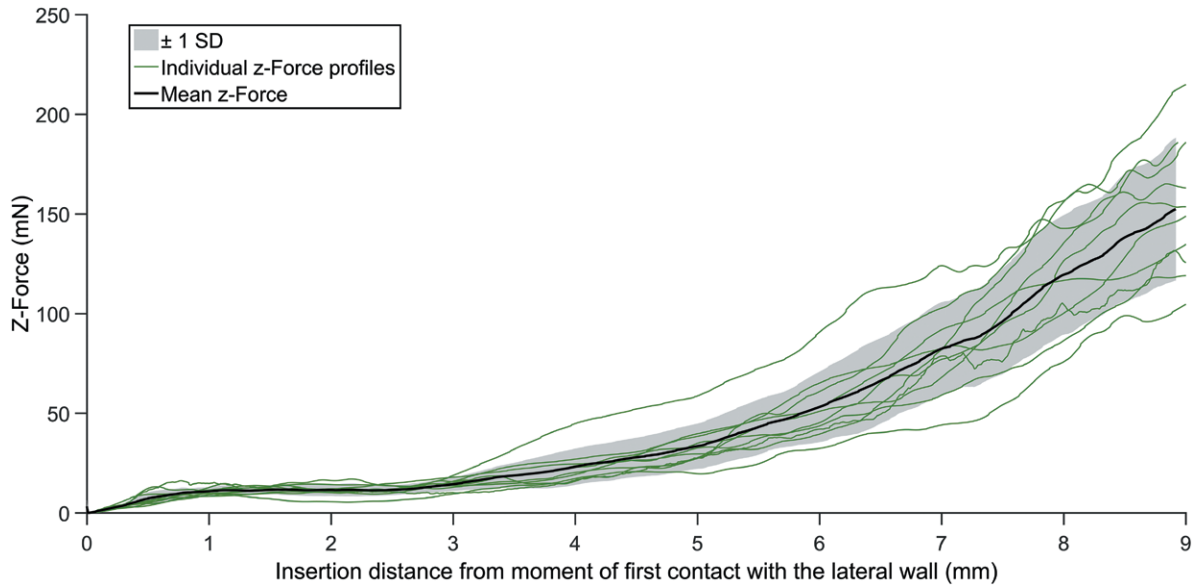


Fig. 5. The mean z force (black) and the individual z forces (green) as a function of the insertion distance from the moment of the initial contact of the electrode tip and the lateral wall. The gray area indicates ± 1 SD. The electrode array was inserted with a constant speed of 0.5 mm/s. The forces follow a similar pattern until 12.8 mm from the round window and start to rise with different ascent.

cochlear geometry had a significant impact on the electrode array insertion forces and possible insertion trauma. The force profile allowed identifying the buckling of an electrode in the cochlea.

In previous studies, a large variability in cochlear form was observed (Zrunek et al. 1980; Wysocki 1999; Escudé et al. 2006; Erixon et al. 2009; Biedron et al. 2010; Verbist et al.

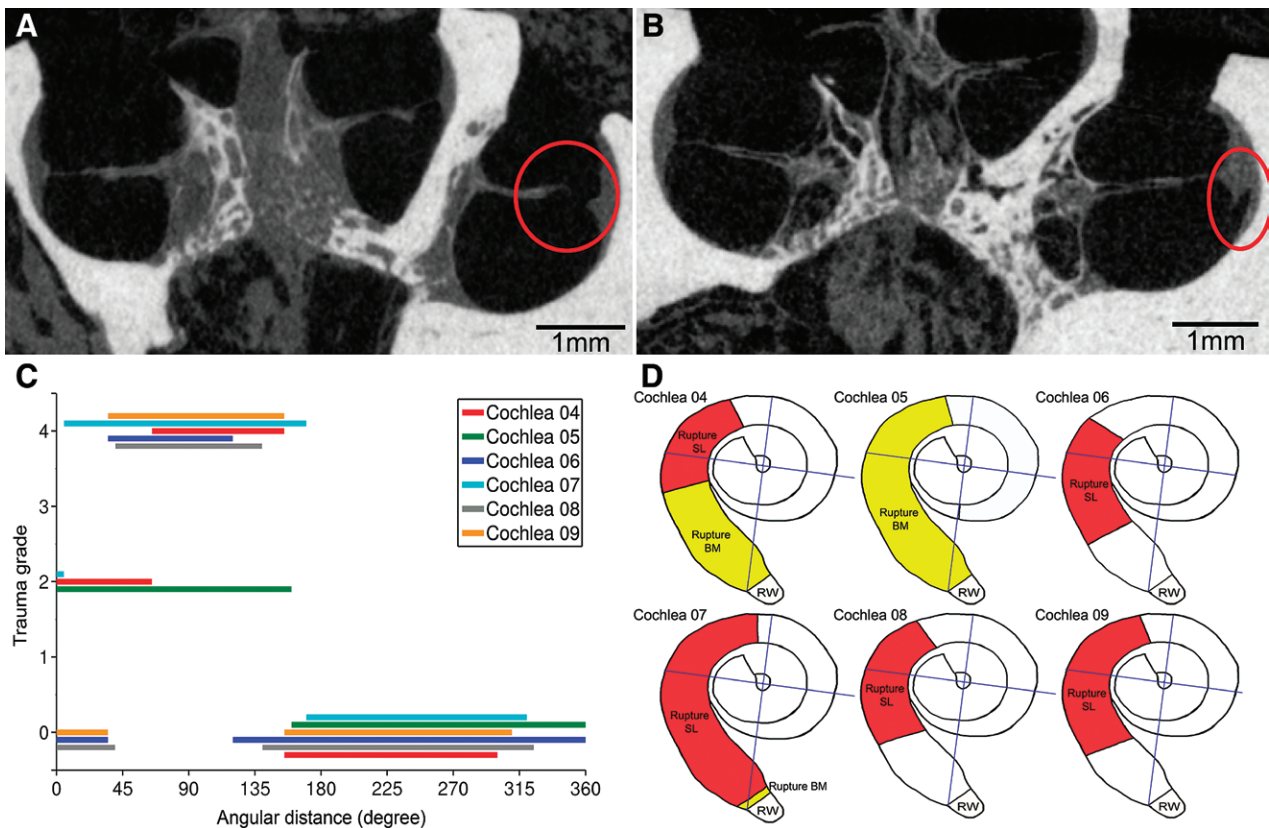


Fig. 6. The micro-CT image of a microdissected cochlea (resolution: 10 μ m) (A and B). A, Trauma to the BM at the basal part of the cochlea, whereby the BM was detached from the SL. B, Trauma to the SL at the basal part of the cochlea, where the damage was in form of tears. C, The grade of trauma as a function of the angular distance. Trauma occurred frequently at the basal part of the cochlea, with trauma to the BM (grade 2) or SL (grade 4). D, A schematic representation of the cochleae to visualize the angular position of the insertion trauma. The red area represents SL rupture (grade 4), and the yellow area shows BM rupture (grade 2). BM indicates basilar membrane; CT, computed tomography; SL, spiral lamina; RW, round window.

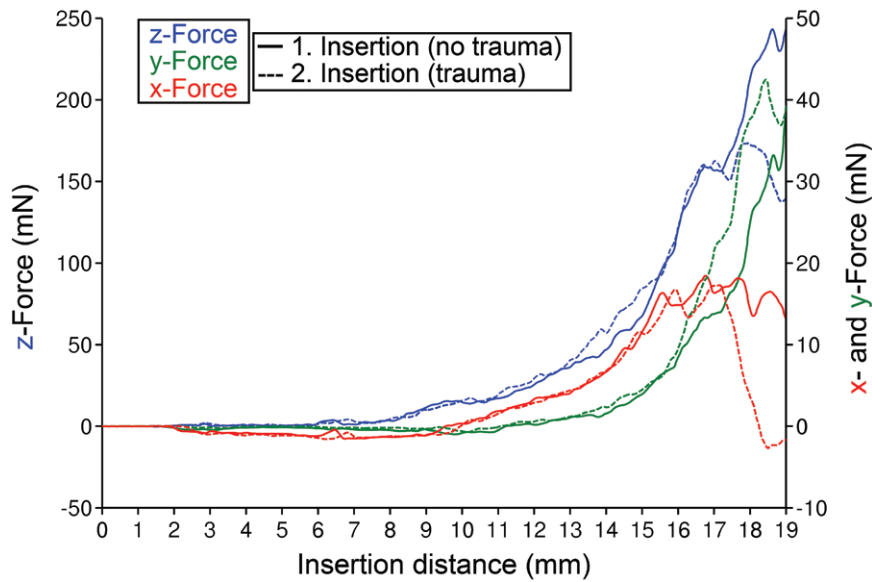


Fig. 7. The difference in force profiles in case of insertion with and without trauma. Insertion forces were plotted against the insertion distance from the round window. Solid lines represent the first insertion without trauma, and dotted lines the second insertion with trauma. At the time of trauma, the z forces stopped to increase, and the slope of the y force was higher compared with the first insertion. The x force shows a prominent drop during the trauma.

2010; Rask-Andersen et al. 2011; Erixon & Rask-Andersen 2013; Shin et al. 2013), and suggested that the electrode insertion and the procedure should be adjusted to the individual cochlear anatomy (Erixon & Rask-Anderson 2013; Avci et al. 2014; Breinbauer & Praetorius 2015; Singla et al. 2015). The present study provides direct experimental support for such a claim.

Several studies investigated forces during insertion of CI electrode arrays into artificial ST models, cadaveric temporal bones, or computational models (Adunka et al. 2004; Roland 2005; Adunka & Kiefer 2006; Zhang et al. 2006, 2009; Todd 2007; Radeloff et al. 2009; Majdani et al. 2010; Rau et al. 2010; Schurzig et al. 2010; Helbig et al. 2011; Kontorinis et al. 2011; Miroir et al. 2012; Nguyen et al. 2012; Kobler et al. 2014, 2015; Rohani et al. 2014; Wade et al. 2014; Gwon et al. 2015). In all previous studies, electrode array insertion was recorded only in one axis (insertion direction). The ST represents, however, a spiral-shaped bony canal. Reducing the forces to one-dimension unrealistically simplifies the mechanical behavior of an electrode array during insertion. As the present study demonstrates, adding x- and y- forces into the analysis allows a superior assessment of the danger of cochlear damage compared with one-dimensional measurements. However, even the 3D force profile alone did not allow an unequivocal identification of cochlear trauma in each case. It requires mentioning that the FMS records the total force in three directions that are applied on the load cell. The forces in

each direction are a sum of the forces the electrode array exerts at each electrode contact point. Consequently, local (opposite) forces might cancel each other. This may prevent detecting some forms of trauma.

The microdissection of the cochlea enabled us to directly observe the mechanical behavior of the electrode array inside of the ST. Similar microdissections did not affect the forces significantly compared with an intact cochlea (Nguyen et al. 2012). Micro-CT allowed highly precise measurements of the cochlear dimensions (max. measurement error: 20 μm). Micro-CT is therefore a suitable tool to evaluate intracochlear mechanical trauma after electrode array insertion. Although histology allows for better visualization of cellular intracochlear structures and reveals also a trauma limited to cells, it investigates the cochlea in the cutting direction, usually midmodiolar plane. Micro-CT allows a nondestructive visualization of the integrity of the membranous and osseous structures in a precise 3D configuration. The insertion trauma can thus be easily located at any place of the cochlea, provided it is sufficiently large and on tissue that is observable in micro-CT. Owing to the high resolution (10 μm) and high contrast, trauma to the BM, or SL could be well analyzed in this and previous studies (Postnov et al. 2006; Teymouri et al. 2011; Frisch et al. 2015).

However, a limitation of the present study was that the RW had to be slightly enlarged to avoid external contact between the electrode array and the RW opening, which could affect the recorded insertion forces. This intervention makes the insertions not fully

TABLE 2. Mean forces before (B) and during trauma (D) for both insertions

		B		D		B		D		B		D	
Trauma		F_x (mN)		F_y (mN)		F_z (mN)		F_{TOT} (mN)					
Insertion 1	No	5.5	16.1	2.2	23.9	46.4	203.4	46.9	205.5				
Insertion 2	Yes	5.2	5.4	2.9	33.8	49.8	159.3	50.3	163.2				

The deviation between the first and second insertion increase after trauma occurs. F_x : x force; F_y : y force; F_z : z force; F_{TOT} : total force.

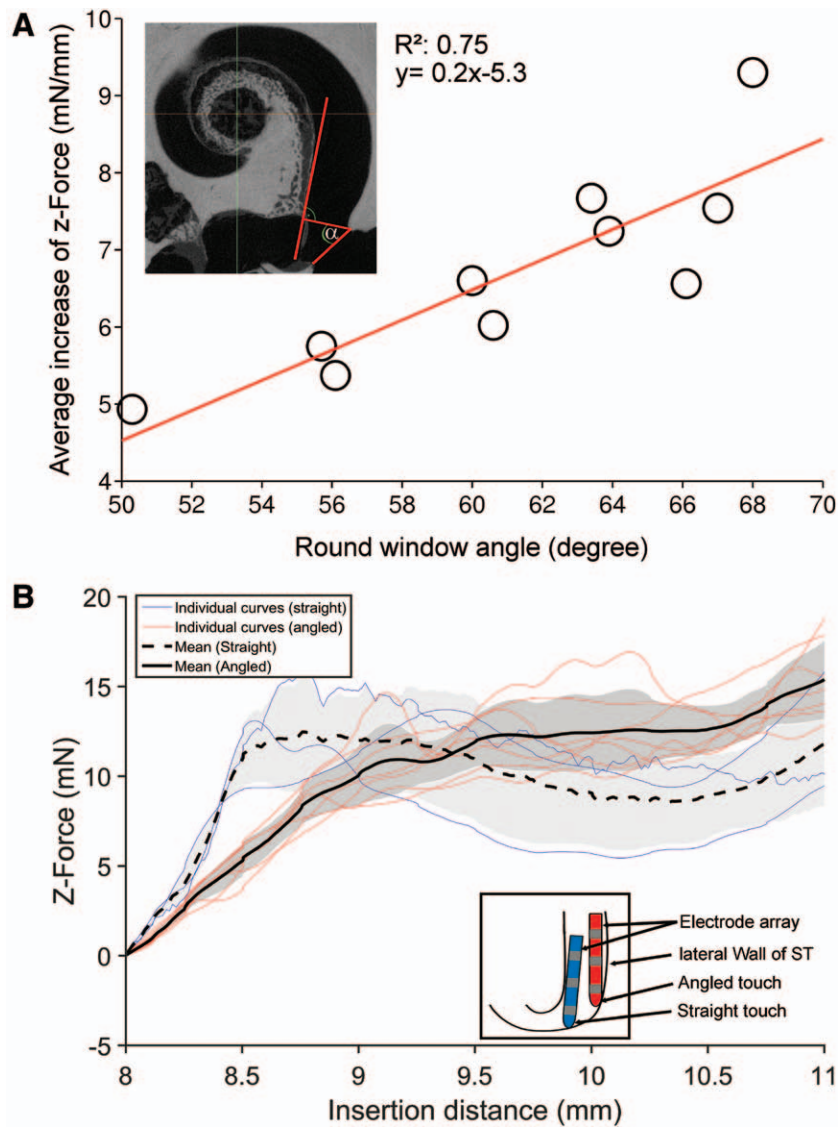


Fig. 8. A, Correlation between round window angle and average increase of the z force between initial contact and 180° from the round window. The average increase of the z force was calculated based on the difference in z force every 1 mm. B, The graph illustrates the average and the individual raise in z force (for an angled and a straight touch of the electrode tip) as a function of the insertion distance. The gray vertical lines indicate ± 1 SD. Bottom right, Schematic representation of the initial contact between the electrode tip and the lateral wall to visualize the difference between the angled and straight touch. The slope of the straight touch was twice as high as the angled touch.

representative of a pure RW insertion, but rather of an extended RW insertion. A further limitation of the present technique was the removal of the electrode array prior micro-CT scanning (to avoid imaging artifacts). Despite maximal care during explantation, additional intracochlear damage during electrode removal cannot be excluded.

The achieved insertion depth in this study was not typical of in vivo condition where insertions are deeper. Cadaveric temporal bones are less hydrated, and the intracochlear soft tissues are stiffer compared with in vivo soft tissue, which leads to increased insertion resistance and somewhat higher friction forces (Roland et al. 2005; Mukherjee et al. 2012). Due to the cadaveric temporal bones used in this study, the recorded insertion forces are therefore likely to be higher than the forces attained in vivo.

The basic measurements obtained using micro-CT showed the mean length of the cochlear base (length *A*: 9.35 ± 0.31 mm) and

the mean width of the cochlear base (width *B*: 7.04 ± 0.34 mm) in accordance with previous reports (length *A*: 9.1 to 9.3 mm; width *B*: 6.8 to 7.0 mm; Escudé et al. 2006; Erixon et al. 2009; Erixon & Rask-Andersen 2013; Avci et al. 2014). Dividing the cochlea in four quadrants allowed better interpretation of the interindividual variability of the human cochlea on temporary insertion forces. The cochlear parameters used in this study to investigate relations to the cochlear trauma can be also determined with conventional CTs, and therefore applicable in living subject prior surgery.

Three-Dimensional Force Measurements

The 3D FMS combined with an automated mechanical insertion allowed us to achieve similar insertion forces with multiple insertions using one electrode array in one human cochlea. The electrode array we used in the present study showed that

repeated insertions showed small variability and the mechanics of the electrode array did not change substantially. Furthermore, due to the low coefficient of variation (<12%), the mean insertion forces over three trials can be considered as a characteristic force profile of a cochlea, whereby automated insertions show less variability compared with manual insertions (Majdani et al. 2010; Kobler et al. 2015; Todt et al. 2016).

Our observation of the trajectory of the electrode array in a fresh-frozen cochlea is in accordance with previous studies on ST models, cadaveric temporal bones, and computational models (Chen et al. 2003; Roland 2005; Miroir et al. 2012; Nguyen et al. 2012). The resulting forces between the electrode array and the lateral wall of the ST have been mathematically described previously and were in a similar range (Roland 2005; Todd 2007; Zou et al. 2015). The electrode array insertion represents a mixture of moving parallel to and pushing against the lateral wall. It is important to note that the force profiles of all cochleae showed similar patterns in x , y , and z direction as long as (intracochlear) buckling was not observed. The z force exerted the highest amount of force, which buildup with increasing contact (friction) between the electrode array and the lateral wall as the array moved forward. When the electrode array started to bend around the modiolus (on average starting at $197^\circ \pm 25^\circ$ from the RW), the anatomy of the cochlea started to influence the profile of the x and z force. This result is in accordance with previous studies, where an increase of the forces occurred between 180° and 200° , or beyond 200° (Lim et al. 2005; Miroir et al. 2012; Nguyen et al. 2012).

Typically, the electrode array can only advance when the advancing force is larger than the opposing frictional force (Zou et al. 2015). To achieve a complete insertion, the insertion force should be in the range of the critical buckling load of the electrode array. A greater portion of the advanced force is spent overcoming frictional forces between the electrode array and the lateral wall while the electrode array is inserted further. If the frictional force is larger and prevents the electrode tip from moving, then the proximal section of the electrode array starts to buckle due to the array stiffness. In case of buckling, a sudden change of the x and y forces was observed, and the z force started to increase. However, the change of the z force was less characteristic for buckling than the drop of the x force or the rise of the y force.

Because the z force almost constantly increases through the whole insertion, the change of the z force is not sufficient to detect electrode buckling. Such detection requires the recording of x and y forces.

Insertion Trauma

Several factors are related to intracochlear trauma during electrode insertion, including cochlear anatomy, condition of the intracochlear structures, electrode stiffness (in vertical and horizontal direction), fluid displacement of the perilymph, and the surgical approach.

In the present study, trauma identification was possible in 7 of 10 cochlea, where the remaining 3 cochleae had to be excluded because of fixation and scanning issues. Regarding insertion forces, we have detected a correlate of the trauma, but not the trauma itself: we observed changes in force profiles in cases when buckling of the electrode array occurred. Referring to this, insertion trauma occurred in six of seven cochleae, frequently at the basal part of the cochlea. The basal part of the

cochlea thus represents a critical region for implantation, where buckling of the electrode array, most likely at its proximal part, increases the risk of trauma to the cochlear structures (BM, OSL). Intracochlear buckling did not result in higher forces on the contrary: if the electrode array was pushed toward the SV, the total insertion force dropped: the forces in x and z direction decreased during trauma, and only the vertical force significantly increased. As a result, in a real condition, the surgeon would most probably not feel any obstruction (it at all, than the contrary) and would consequently not stop the insertion process. The fact that intracochlear trauma caused by buckling cannot be detected by the surgeon is thus one implication of the present measurements.

Rupturing of the SL occurred in six cochleae, BM rupture in three of seven cochleae. The cochlear trauma was exclusive: if damage to the BM occurred no damage to the SL was observed, and vice versa. Thus, once a certain trauma occurs, it likely releases the stress from the electrode and prevents trauma elsewhere. In the present study, the maximal x forces were 2.5 times higher in cochleae with SL trauma (table not included), meaning that a significant higher pressure against the SL at the base of the cochlea might cause a trauma.

Trauma to the BM and SL represents the most common cochlear injury with 25 to 43% (Shepherd et al. 1985; Kennedy 1987; Adunka et al. 2004; Adunka & Kiefer 2006; Skarzynski & Podskarbi-Fayette 2010; Wimmer et al. 2014). Where damage to the BM obviously affects acoustic hearing directly, previous studies reported that the SL as well plays a key role in the maintenance of the ionic environment and the endocochlear potential (Schulte & Adams 1989; Crouch et al. 1997). Hearing loss occurs following the loss of fibrocytes in the cochlear lateral wall (Hoya et al. 2004), particularly in the SL, where potassium recycling takes place. A damage of the presumed recycling pathway may cause hearing loss similar to the connexin mutations, targeting the same pathway (Hibino & Kurachi 2006). Finally, the vascular supply to the stria might be affected by a mechanical forces acting on the SL. In our study, the initial contact between the electrode array and the lateral wall was $121^\circ \pm 9^\circ$, whereas SL trauma started between 13° and 59° from the RW. Consequently, the middle and the proximal part of the electrode array are most likely responsible for trauma to the SL, and not the electrode tip. The situation may differ in cases of deeper insertions or other electrodes not studied here. It needs to be emphasized that the present data are only reflecting one electrode with the given size and stiffness.

Intracochlear trauma at 180° from the RW was frequently reported in previous studies (O'Leary et al. 1991; Nadol et al. 1994, 2001; Richter et al. 2001; Tykocinski et al. 2001; Aschen-dorff et al. 2003; Eshraghi et al. 2003; Roland 2005; Wardrop et al. 2005; Finley & Skinner 2008; Wanna et al. 2011), however, in the present study there was no such trauma at 180° . A difference to the previous studies is that due to the clear view of the ST trajectory in a microdissected cochlea, the best suitable insertion vector could be determined before implantation in the present experiments, as we were able to rotate the cochlea in the most favorable angle. McRackan et al. (2013) used an image-guided trajectory, and also noted no trauma at 180° from the RW. Combining this with the present data indicates that a correct insertion angle in y direction reduces the risk of electrode dislocation near 180° and thus also the risk of a tip-induced trauma.

Correlation Between Cochlear Geometry and Force Profile

Previous studies have shown that size, location, angle, and the accessibility of the RW has a large effect on implantation outcomes (Kha et al. 2007; Li et al. 2007; Roland et al. 2007; Meshik et al. 2010; Adunka et al. 2010; Shapira et al. 2011; Gibson et al. 2012; Wimmer et al. 2014; Breinbauer & Praetorius 2015; Zou et al. 2015). We found a statistically significant correlation between RW angle and the local friction force. A large RW angle (Fig. 8A) resulted in bending of the electrode array around the RW entrance and directed the electrode array against the modiolum. Consequently, the electrode tip was sliding along the modiolar wall on the way to its initial contact with the lateral wall of the basal part, which was visible on the force profiles (max: 10 mN). However, trauma identification using micro-CT has not revealed any damage to the modiolar wall due to the electrode tip, meaning that those forces exerted to the modiolar wall in the present setup were too small to induce visible trauma to the spongy bone covering the modiolum. Although potentially increasing the risk of trauma (Zou et al. 2015), we have not seen any correlated translocations or trauma with unfavorable insertion angles.

ACKNOWLEDGMENTS

This research was supported by Advanced Bionics and the German Research Foundation (DFG; Cluster of Excellence Hearing4all).

The authors have no conflicts of interest to disclose.

Address correspondence to Ersin Avci, Cluster of Excellence Hearing4all, Institute of AudioNeuroTechnology and Department of Experimental Otolaryngology, ENT Clinics, Hannover Medical School, Stadtfeldamm 34, 30625 Hannover, Germany. E-mail: avci.ersin84@gmail.com

Received June 13, 2016; accepted October 19, 2016.

REFERENCES

- Adunka, O., & Kiefer, J. (2006). Impact of electrode insertion depth on intracochlear trauma. *Otolaryngol Head Neck Surg*, *135*, 374–382.
- Adunka, O., Kiefer, J., Unkelbach, M. H., et al. (2004). Development and evaluation of an improved cochlear implant electrode design for electric acoustic stimulation. *Laryngoscope*, *114*, 1237–1241.
- Adunka, O. F., Pillsbury, H. C., Buchman, C. A. (2010). Minimizing intracochlear trauma during cochlear implantation. *Adv Otorhinolaryngol*, *67*, 96–107.
- Aschendorff, A., Klenzner, T., Richter, B., et al. (2003). Evaluation of the HiFocus electrode array with positioner in human temporal bones. *J Laryngol Otol*, *117*, 527–531.
- Aschendorff, A., Kromeier, J., Klenzner, T., et al. (2007). Quality control after insertion of the nucleus contour and contour advance electrode in adults. *Ear Hear*, *28*(2 Suppl), 75S–79S.
- Avci, E., Nauwelaers, T., Lenarz, T., et al. (2014). Variations in microanatomy of the human cochlea. *J Comp Neurol*, *522*, 3245–3261.
- Biedron, S., Prescher, A., Ilgner, J., et al. (2010). The internal dimensions of the cochlear scalae with special reference to cochlear electrode insertion trauma. *Otol Neurotol*, *31*, 731–737.
- Breinbauer, H. A., & Praetorius, M. (2015). Variability of an ideal insertion vector for cochlear implantation. *Otol Neurotol*, *36*, 610–617.
- Briggs, R. J., Tykocinski, M., Lazsig, R., et al. (2011). Development and evaluation of the modiolar research array—multi-centre collaborative study in human temporal bones. *Cochlear Implants Int*, *12*, 129–139.
- Chen, B. K., Clark, G. M., Jones, R. (2003). Evaluation of trajectories and contact pressures for the straight nucleus cochlear implant electrode array - a two-dimensional application of finite element analysis. *Med Eng Phys*, *25*, 141–147.
- Crouch, J. J., Sakaguchi, N., Lytle, C., et al. (1997). Immunohistochemical localization of the Na-K-Cl co-transporter (NKCC1) in the gerbil inner ear. *J Histochem Cytochem*, *45*, 773–778.
- Erixon, E., & Rask-Andersen, H. (2013). How to predict cochlear length before cochlear implantation surgery. *Acta Otolaryngol*, *133*, 1258–1265.
- Erixon, E., Högstorp, H., Wadin, K., et al. (2009). Variational anatomy of the human cochlea: Implications for cochlear implantation. *Otol Neurotol*, *30*, 14–22.
- Escudé, B., James, C., Deguine, O., et al. (2006). The size of the cochlea and predictions of insertion depth angles for cochlear implant electrodes. *Audiol Neurootol*, *11*(Suppl 1), 27–33.
- Eshraghi, A. A., Yang, N. W., Balkany, T. J. (2003). Comparative study of cochlear damage with three perimodiolar electrode designs. *Laryngoscope*, *113*, 415–419.
- Finley, C. C., Holden, T. A., Holden, L. K., et al. (2008). Role of electrode placement as a contributor to variability in cochlear implant outcomes. *Otol Neurotol*, *29*, 920–928.
- Franke-Trieger, A., Jolly, C., Darbinjan, A., et al. (2014). Insertion depth angles of cochlear implant arrays with varying length: a temporal bone study. *Otol Neurotol*, *35*, 58–63.
- Frisch, T., Bloch, S. L., Sørensen, M. S. (2015). Prevalence, size and distribution of microdamage in the human otic capsule. *Acta Otolaryngol*, *135*, 771–775.
- Gantz, B. J., & Turner, C. (2004). Combining acoustic and electrical speech processing: Iowa/Nucleus hybrid implant. *Acta Otolaryngol*, *124*, 344–347.
- Gibson, D., Gluth, M. B., Whyte, A., et al. (2012). Rotation of the osseous spiral lamina from the hook region along the basal turn of the cochlea: results of a magnetic resonance image anatomical study using high-resolution DRIVE sequences. *Surg Radiol Anat*, *34*, 781–785.
- Gwon, T. M., Min, K. S., Kim, J. H., et al. (2015). Fabrication and evaluation of an improved polymer-based cochlear electrode array for atraumatic insertion. *Biomed Microdevices*, *17*, 32.
- Helbig, S., Settevendemie, C., Mack, M., et al. (2011). Evaluation of an electrode prototype for atraumatic cochlear implantation in hearing preservation candidates: Preliminary results from a temporal bone study. *Otol Neurotol*, *32*, 419–423.
- Hibino, H., & Kurachi, Y. (2006). Molecular and physiological bases of the K⁺ circulation in the mammalian inner ear. *Physiology (Bethesda)*, *21*, 336–345.
- Hoya, N., Okamoto, Y., Kamiya, K., et al. (2004). A novel animal model of acute cochlear mitochondrial dysfunction. *Neuroreport*, *15*, 1597–1600.
- Kawano, A., Seldon, H. L., Clark, G. M. (1996). Computer-aided three-dimensional reconstruction in human cochlear maps: measurement of the lengths of organ of Corti, outer wall, inner wall, and Rosenthal's canal. *Ann Otol Rhinol Laryngol*, *105*, 701–709.
- Kennedy, D. W. (1987). Multichannel intracochlear electrodes: Mechanism of insertion trauma. *Laryngoscope*, *97*, 42–49.
- Kha, H. N., Chen, B. K., Clark, G. M. (2007). 3D finite element analyses of insertion of the Nucleus standard straight and the Contour electrode arrays into the human cochlea. *J Biomech*, *40*, 2796–2805.
- Kiefer, J., Pok, M., Adunka, O., et al. (2005). Combined electric and acoustic stimulation of the auditory system: Results of a clinical study. *Audiol Neurootol*, *10*, 134–144.
- Kobler, J. P., Beckmann, D., Rau, T. S., et al. (2014). An automated insertion tool for cochlear implants with integrated force sensing capability. *Int J Comput Assist Radiol Surg*, *9*, 481–494.
- Kobler, J. P., Dhanasingh, A., Kiran, R., et al. (2015). Cochlear dummy electrodes for insertion training and research purposes: Fabrication, mechanical characterization, and experimental validation. *Biomed Res Int*, *2015*, 574209.
- Kontorinis, G., Lenarz, T., Stöver, T., et al. (2011). Impact of the insertion speed of cochlear implant electrodes on the insertion forces. *Otol Neurotol*, *32*, 565–570.
- Lenarz, T. (2009). Electro-acoustic stimulation of the cochlea. Editorial. *Audiol Neurootol*, *14*(Suppl 1), 1.
- Li, P. M., Wang, H., Northrop, C., et al. (2007). Anatomy of the round window and hook region of the cochlea with implications for cochlear implantation and other endocochlear surgical procedures. *Otol Neurotol*, *28*, 641–648.
- Lim, Y. S., Park, S. I., Kim, Y. H., et al. (2005). Three-dimensional analysis of electrode behavior in a human cochlear model. *Med Eng Phys*, *27*, 695–703.

- Majdani, O., Schurzig, D., Hussong, A., et al. (2010). Force measurement of insertion of cochlear implant electrode arrays *in vitro*: Comparison of surgeon to automated insertion tool. *Acta Otolaryngol*, *130*, 31–36.
- McRackan, T. R., Balachandran, R., Blachon, G. S., et al. (2013). Validation of minimally invasive, image-guided cochlear implantation using Advanced Bionics, Cochlear, and Medel electrodes in a cadaver model. *Int J Comput Assist Radiol Surg*, *8*, 989–995.
- Meshik, X., Holden, T. A., Chole, R. A., et al. (2010). Optimal cochlear implant insertion vectors. *Otol Neurotol*, *31*, 58–63.
- Miroir, M., Nguyen, Y., Kazmitcheff, G., et al. (2012). Friction force measurement during cochlear implant insertion: Application to a force-controlled insertion tool design. *Otol Neurotol*, *33*, 1092–1100.
- Mukherjee, P., Uzun-Coruhlu, H., Wong, C. C., et al. (2012). Assessment of intracochlear trauma caused by the insertion of a new straight research array. *Cochlear Implants Int*, *13*, 156–162.
- Nadol, J. B., Jr, Ketten, D. R., Burgess, B. J. (1994). Otopathology in a case of multichannel cochlear implantation. *Laryngoscope*, *104*(3 Pt 1), 299–303.
- Nadol, J. B., Jr, Shiao, J. Y., Burgess, B. J., et al. (2001). Histopathology of cochlear implants in humans. *Ann Otol Rhinol Laryngol*, *110*, 883–891.
- Nguyen, Y., Miroir, M., Kazmitcheff, G., et al. (2012). Cochlear implant insertion forces in microdissected human cochlea to evaluate a prototype array. *Audiol Neurootol*, *17*, 290–298.
- O'Leary, M. J., Fayad, J., House, W. F., et al. (1991). Electrode insertion trauma in cochlear implantation. *Ann Otol Rhinol Laryngol*, *100*(9 Pt 1), 695–699.
- Postnov, A., Zarowski, A., De Clerck, N., et al. (2006). High resolution micro-CT scanning as an innovative tool for evaluation of the surgical positioning of cochlear implant electrodes. *Acta Otolaryngol*, *126*, 467–474.
- Radeloff, A., Unkelbach, M. H., Mack, M. G., et al. (2009). A coated electrode carrier for cochlear implantation reduces insertion forces. *Laryngoscope*, *119*, 959–963.
- Rask-Andersen, H., Erixon, E., Kinnefors, A., et al. (2011). Anatomy of the human cochlea—implications for cochlear implantation. *Cochlear Implants Int*, *12*(Suppl 1), S8–13.
- Rau, T. S., Hussong, A., Leinung, M., et al. (2010). Automated insertion of preformed cochlear implant electrodes: Evaluation of curling behaviour and insertion forces on an artificial cochlear model. *Int J Comput Assist Radiol Surg*, *5*, 173–181.
- Ravicz, M. E., Merchant, S. N., Rosowski, J. J. (2000). Effect of freezing and thawing on stapes-cochlear input impedance in human temporal bones. *Hear Res*, *150*, 215–224.
- Richter, B., Aschendorff, A., Lohnstein, P., et al. (2001). The Nucleus Contour electrode array: A radiological and histological study. *Laryngoscope*, *111*, 508–514.
- Rohani, P., Pile, J., Kahrs, L. A., et al. (2014). Forces and trauma associated with minimally invasive image-guided cochlear implantation. *Otolaryngol Head Neck Surg*, *150*, 638–645.
- Roland, J. T., Jr. (2005). A model for cochlear implant electrode insertion and force evaluation: Results with a new electrode design and insertion technique. *Laryngoscope*, *115*, 1325–1339.
- Roland, P. S., Wright, C. G., Isaacson, B. (2007). Cochlear implant electrode insertion: The round window revisited. *Laryngoscope*, *117*, 1397–1402.
- Rosowski, J. J., Davis, P. J., Merchant, S. N., et al. (1990). Cadaver middle ears as models for living ears: Comparisons of middle ear input impedance. *Ann Otol Rhinol Laryngol*, *99*(5 Pt 1), 403–412.
- Schulte, B. A., & Adams, J. C. (1989). Distribution of immunoreactive Na⁺, K⁺-ATPase in gerbil cochlea. *J Histochem Cytochem*, *37*, 127–134.
- Schurzig, D., Webster, R. J. III, Dietrich, M. S., et al. (2010). Force of cochlear implant electrode insertion performed by a robotic insertion tool: Comparison of traditional versus Advance Off-Stylet techniques. *Otol Neurotol*, *31*, 1207–1210.
- Schuster, D., Kratchman, L. B., Labadie, R. F. (2015). Characterization of intracochlear rupture forces in fresh human cadaveric cochleae. *Otol Neurotol*, *36*, 657–661.
- Shapira, Y., Eshraghi, A. A., Balkany, T. J. (2011). The perceived angle of the round window affects electrode insertion trauma in round window insertion - an anatomical study. *Acta Otolaryngol*, *131*, 284–289.
- Shepherd, R. K., Clark, G. M., Pyman, B. C., et al. (1985). Banded intracochlear electrode array: Evaluation of insertion trauma in human temporal bones. *Ann Otol Rhinol Laryngol*, *94*(1 Pt 1), 55–59.
- Shin, K. J., Lee, J. Y., Kim, J. N., et al. (2013). Quantitative analysis of the cochlea using three-dimensional reconstruction based on microcomputed tomographic images. *Anat Rec (Hoboken)*, *296*, 1083–1088.
- Singla, A., Sahni, D., Gupta, A. K., et al. (2015). Surgical anatomy of the basal turn of the human cochlea as pertaining to cochlear implantation. *Otol Neurotol*, *36*, 323–328.
- Skarzynski, H., & Podskarbi-Fayette, R. (2010). A new cochlear implant electrode design for preservation of residual hearing: A temporal bone study. *Acta Otolaryngol*, *130*, 435–442.
- Teymouri, J., Hullar, T. E., Holden, T. A., et al. (2011). Verification of computed tomographic estimates of cochlear implant array position: A micro-CT and histologic analysis. *Otol Neurotol*, *32*, 980–986.
- Todd, C. A., Naghdy, F., Svehla, M. J. (2007). Force application during cochlear implant insertion: An analysis for improvement of surgeon technique. *IEEE Trans Biomed Eng*, *54*, 1247–1255.
- Todt, I., Ernst, A., Mittmann, P. (2016). Effects of different insertion techniques of a cochlear implant electrode on the intracochlear pressure. *Audiol Neurootol*, *21*, 30–37.
- Tykocinski, M., Saunders, E., Cohen, L. T., et al. (2001). The contour electrode array: Safety study and initial patient trials of a new perimodiolar design. *Otol Neurotol*, *22*, 33–41.
- Verbist, B. M., Skinner, M. W., Cohen, L. T., et al. (2010). Consensus panel on a cochlear coordinate system applicable in histologic, physiologic, and radiologic studies of the human cochlea. *Otol Neurotol*, *31*, 722–730.
- von Ilberg, C., Kiefer, J., Tillein, J., et al. (1999). Electric-acoustic stimulation of the auditory system. New technology for severe hearing loss. *ORL J Otorhinolaryngol Relat Spec*, *61*, 334–340.
- Wade, S. A., Fallon, J. B., Wise, A. K., et al. (2014). Measurement of forces at the tip of a cochlear implant during insertion. *IEEE Trans Biomed Eng*, *61*, 1177–1186.
- Wanna, G. B., Noble, J. H., McRackan, T. R., et al. (2011). Assessment of electrode placement and audiological outcomes in bilateral cochlear implantation. *Otol Neurotol*, *32*, 428–432.
- Wanna, G. B., Noble, J. H., Carlson, M. L., et al. (2014). Impact of electrode design and surgical approach on scalar location and cochlear implant outcomes. *Laryngoscope*, *124*(Suppl 6), S1–S7.
- Wardrop, P., Winney, D., Rebscher, S. J., et al. (2005). A temporal bone study of insertion trauma and intracochlear position of cochlear implant electrodes. I: Comparison of Nucleus banded and Nucleus Contour electrodes. *Hear Res*, *203*, 54–67.
- Wimmer, W., Bell, B., Huth, M. E., et al. (2014). Cone beam and micro-computed tomography validation of manual array insertion for minimally invasive cochlear implantation. *Audiol Neurootol*, *19*, 22–30.
- Wysocki, J. (1999). Dimensions of the human vestibular and tympanic scalae. *Hear Res*, *135*, 39–46.
- Zhang, J., Xu, K., Simaan, N., et al. (2006). A pilot study of robot-assisted cochlear implant surgery using steerable electrode arrays. *Med Image Comput Comput Assist Interv*, *9*(Pt 1), 33–40.
- Zhang, J., Bhattacharyya, S., Simaan, N. (2009). Model and parameter identification of friction during robotic insertion of cochlear-implant electrode arrays. *IEEE Int Conf of Rob and Autom*, 3859–3864.
- Zou, J., Lähelmä, J., Koivisto, J., et al. (2015). Imaging cochlear implantation with round window insertion in human temporal bones and cochlear morphological variation using high-resolution cone beam CT. *Acta Otolaryngol*, *135*, 466–472.
- Zrunek, M., & Lischka, M. (1981). Dimensions of the scala vestibuli and sectional areas of both scales. *Arch Otorhinolaryngol*, *233*, 99–104.
- Zrunek, M., Lischka, M., Hochmair-Desoyer, I., et al. (1980). Dimensions of the scala tympani in relation to the diameters of multichannel electrodes. *Arch Otorhinolaryngol*, *229*, 159–165.